

# A SPARSE BAYESIAN LEARNING ALGORITHM FOR ESTIMATION OF INTERACTION KERNELS IN MOTSCH-TADMOR MODEL

JINCHAO FENG\* AND SUI TANG†

**Abstract.** In this paper, we investigate the data-driven identification of asymmetric interaction kernels in the Motsch–Tadmor model based on observed trajectory data. The model under consideration is governed by a class of semilinear evolution equations, where the interaction kernel defines a normalized, state-dependent Laplacian operator that governs collective dynamics. To address the resulting nonlinear inverse problem, we propose a variational framework that reformulates kernel identification using the implicit form of the governing equations, reducing it to a subspace identification problem. We establish an identifiability result that characterizes conditions under which the interaction kernel can be uniquely recovered up to scale. To solve the inverse problem robustly, we develop a sparse Bayesian learning algorithm that incorporates informative priors for regularization, quantifies uncertainty, and enables principled model selection. Extensive numerical experiments on representative interacting particle systems demonstrate the accuracy, robustness, and interpretability of the proposed framework across a range of noise levels and data regimes.

**1. Introduction.** Interacting dynamical systems are ubiquitous in natural and engineered systems, characterized by complex behaviors that emerge from local interactions and the temporal evolution of multiple agents or particles. Examples include planetary orbits, self-propelled motion, bird flocking, fish schooling, cell aggregation, opinion formation, and oscillator synchronization [1, 12, 13, 22, 25, 37, 47]. Differential equation models have been instrumental in understanding how collective behaviors arise from individual interactions. However, the high dimensionality and heterogeneous interaction mechanisms inherent to these systems pose major challenges for mathematical modeling and data-driven learning [28–30, 33].

Recent advances in applied mathematics demonstrate that even simple interaction laws can generate complex emergent dynamics when embedded in mechanistic models [4, 5, 10, 43, 49]. Consider a system of  $N$  agents, each defined by a position  $\mathbf{x}_i(t) \in \mathbb{R}^d$ . For first-order dynamics of homogeneous agents, the governing equations are:

$$(1.1) \quad \frac{d\mathbf{x}_i(t)}{dt} = \sum_{j=1}^N a_t(i, j)(\mathbf{x}_j(t) - \mathbf{x}_i(t)),$$

$$(1.2) \quad a_t(i, j) = \frac{\phi(\|\mathbf{x}_j(t) - \mathbf{x}_i(t)\|)}{c_i},$$

where  $a_t(i, j)$  represents the normalized influence of agent  $j$  on agent  $i$ ;  $\phi : \mathbb{R}^+ \rightarrow \mathbb{R}$  is the interaction kernel based on relative distance; and  $c_i$  is a normalization factor. For symmetric models,  $c_i = N$ , while for asymmetric models,  $c_i = \sum_{j=1}^N \phi(\|\mathbf{x}_j(t) - \mathbf{x}_i(t)\|)$ . These models can also be extended to second-order systems.

While symmetric models have been extensively analyzed, they often fail to capture far-from-equilibrium dynamics where interactions are localized and not uniformly distributed. To address this, Motsch and Tadmor introduced an asymmetric formulation [34, 35], generalizing the Krause model [7, 23] for continuous-time opinion dynamics. In this framework, the influence between agents is scaled by their relative distances, eliminating dependence on the number of agents and emphasizing geometric configuration in phase space. Analogous mechanisms appear in recent advances in machine learning, such as graph transformers with non-symmetric attention mechanisms [14], which show improved empirical performance over their symmetric counterparts. Numerical studies [6, 7, 35] have shown that asymmetric models capture phenomena such as local consensus in opinion dynamics [17] and mono- or multi-cluster flocking [15]. Despite their expressiveness, asymmetric models introduce mathematical difficulties due to the absence of conserved quantities (e.g., total momentum), which are central to the analysis of symmetric systems. While recent works [14, 15, 17, 18, 34, 35] have advanced the understanding of emergent dynamics in asymmetric systems, rigorous analysis remains an active research area.

\*School of Sciences, Great Bay University, Dongguan, Guangdong, China (jcfeng@gbu.edu.cn).

†Departments of Mathematics, University of California, Santa Barbara, Isla Vista, CA (suitang@math.ucsb.edu).

A central challenge in qualitative analysis is identifying interaction functions that lead to spontaneous pattern formation or self-organization. Traditionally, interaction potentials were empirically chosen to replicate observed dynamics. However, advancements in data acquisition technologies, such as digital imaging and GPS tracking [21, 31], now enable the collection of density evolution data for large particle ensembles. This raises a critical question: can the underlying interaction laws governing the dynamics be inferred directly from empirical observations? Addressing this requires algorithms that align theoretical models with empirical observations. This paper tackles this challenge by bridging the gap between models and data. While data-driven approaches have extensively studied symmetric models, asymmetric models remain underexplored. This work focuses on filling this gap.

**1.1. Related Works.** Data-driven discovery of dynamical systems using machine learning has emerged as a core theme in scientific computing [4, 5, 8, 10, 11, 16, 20, 27, 38–40, 43, 49], enabling the representation and analysis of complex functional data. These approaches typically formulate a loss functional comprising a data-fidelity term (enforcing consistency with governing equations) and a regularization term (embedding prior knowledge such as sparsity), transforming the learning task into an optimization problem. This paradigm effectively leverages machine learning techniques to tackle high-dimensional challenges.

Despite extensive progress in symmetric models [26, 28–30, 33], data-driven discovery of asymmetric interaction laws remains underexplored. The lack of symmetry leads to a nonlinear inverse problem, precluding the direct application of prior methods and necessitating new theoretical and algorithmic tools. To the best of our knowledge, this paper is the first to address the data-driven discovery of asymmetric models. The asymmetric property introduces a nonlinear inverse problem, rendering previous techniques for symmetric models inapplicable and necessitating new analytical and algorithmic approaches.

The closest related work involves data-driven learning of ODEs with rational right-hand side functions, often used in modeling biological networks [32]. In such cases, the strong or weak form of the ODE results in a nonlinear least squares problem. To linearize this inverse problem, [32] proposed leveraging the implicit form of ODEs, transforming the task into a linear subspace identification problem. While we adopt a similar strategy, it is well-known that subspace identification is highly sensitive to data perturbations. This issue is particularly pronounced in biological modeling, where stochastic observational data introduces variability and impacts solution robustness.

To robustly address the ill-posed nature of the inverse problem, we adopt a sparse Bayesian learning (SBL) framework. This approach not only enables flexible incorporation of prior information (e.g., sparsity or smoothness) but also quantifies uncertainty in model estimates, leading to more interpretable and stable results. While deterministic sparsity-promoting techniques, such as SINDy (Sequentially Least Squares), iterative greedy methods, and gradient-based methods [9, 11, 42, 46], dominate the literature, Bayesian methods remain underexplored [49].

*Contributions.* Our contributions can be summarized as follows:

- We propose a variational learning framework based on the implicit form of the governing ODE, enabling the identification of interaction kernels in asymmetric models via sparse Bayesian inference.
- We introduce a new model selection criterion for identifying relevant basis functions, which we show outperforms standard approaches under various noise conditions.
- We validate the proposed method on multiple synthetic datasets, demonstrating robustness to noise and efficiency in computation.

**2. Problem Formulation.** We begin by formulating the problem of estimating the interaction kernel  $\phi$  from noise-free observational trajectory data. Let the dataset be denoted by  $\mathcal{D}_{M,L} = \{\mathcal{D}^{(m,l)}\}_{m,l=1}^{M,L} := \{\mathbf{x}_i^{(m)}(t_l), \dot{\mathbf{x}}_i^{(m)}(t_l), i = 1, \dots, N\}_{m,l=1}^{M,L}$ , where  $0 = t_1 < \dots < t_L = T$  are observation time instances. Here,  $m$  denotes the trial number, with initial conditions sampled i.i.d. from a probability measure on  $\mathbb{R}^d$ .

We assume that the interaction kernel  $\phi$  lies in the span of a finite set of basis functions  $\mathcal{S} = \{\xi_k\}_{k=1}^K$ , i.e.,  $\phi = \sum_k c_k^{\text{true}} \xi_k$  for coefficients  $\mathbf{c}^{\text{true}} \in \mathbb{R}^K$ .

Multiplying both sides of the normalized ODE (1.1) by the normalization constant  $\sum_{j \in \mathcal{N}_i} \phi(|\mathbf{x}_j - \mathbf{x}_i|)$ ,

we eliminate the denominator and obtain the implicit constraint:

$$(2.1) \quad \sum_{j=1}^N \phi(|\mathbf{x}_j - \mathbf{x}_i|)(\dot{\mathbf{x}}_i - (\mathbf{x}_i - \mathbf{x}_j)) = 0, \quad i = 1, \dots, N.$$

To estimate  $\phi$ , we propose a variational approach that minimizes the empirical loss functional over the unit sphere in  $\mathbb{R}^K$ , enforcing non-trivial solutions:

$$(2.2) \quad \min_{\|\mathbf{c}\|_2=1} \mathcal{E}_{M,L}(\mathbf{c}),$$

where

$$(2.3) \quad \mathcal{E}_{M,L}(\mathbf{c}) := \frac{1}{NML} \sum_{m,l,i=1,1,1}^{M,L,N} \left\| \sum_{j=1}^N \sum_{k=1}^K c_k \xi_k(|\mathbf{x}_j^{(m)}(t_l) - \mathbf{x}_i^{(m)}(t_l)|)(\dot{\mathbf{x}}_i^{(m)}(t_l) - (\mathbf{x}_i^{(m)}(t_l) - \mathbf{x}_j^{(m)}(t_l))) \right\|^2.$$

The goal is to identify a function from the candidate library that satisfies (2.1) as closely as possible on the observed data, ensuring  $\mathcal{E}_{M,L}(\mathbf{c}^{\text{true}}) = 0$ . Since  $\mathcal{E}_{M,L}(\cdot)$  is quadratic in  $\mathbf{c}$ , it admits a closed-form solution described in Proposition 2.1. We note that directly using the original ODE form (1.1) as the loss function leads to a nonlinear least squares problem, which is more challenging to solve.

PROPOSITION 2.1. *Let  $\hat{\mathbf{c}}_{M,L} = \arg \min_{\|\mathbf{c}\|_2=1} \mathcal{E}_{M,L}(\mathbf{c})$ . Then:*

$$(2.4) \quad \frac{1}{NML} \mathbb{A}_{M,L}^T \mathbb{A}_{M,L} \hat{\mathbf{c}}_{M,L} = \mathbf{0},$$

where  $\mathbb{A}_{M,L} = \begin{pmatrix} \mathbf{A}^{(1,1)} \\ \vdots \\ \mathbf{A}^{(M,L)} \end{pmatrix} \in \mathbb{R}^{dNML \times K}$  with  $\mathbf{A}^{(m,l)} = [\mathbf{A}_{ik}^{(m,l)}] \in \mathbb{R}^{dN \times K}$ , and

$$(2.5) \quad \mathbf{A}_{ik}^{(m,l)} = \sum_{j=1}^N \xi_k(|\mathbf{x}_j^{(m)}(t_l) - \mathbf{x}_i^{(m)}(t_l)|)(\dot{\mathbf{x}}_i^{(m)}(t_l) - (\mathbf{x}_i^{(m)}(t_l) - \mathbf{x}_j^{(m)}(t_l))) \in \mathbb{R}^d,$$

for  $i = 1, \dots, N$  and  $k = 1, \dots, K$ .

*Proof.* The loss function  $\mathcal{E}_{M,L}(\mathbf{c})$  can be written as a quadratic form:

$$\mathcal{E}_{M,L}(\mathbf{c}) = \frac{1}{NML} \|\mathbb{A}_{M,L} \mathbf{c}\|^2 = \frac{1}{NML} \mathbf{c}^T \mathbb{A}_{M,L}^T \mathbb{A}_{M,L} \mathbf{c}.$$

Differentiating with respect to  $\mathbf{c}$  and setting it to zero gives:

$$\mathbb{A}_{M,L}^T \mathbb{A}_{M,L} \mathbf{c} = \mathbf{0},$$

which proves the result.  $\square$

The null spaces of  $\mathbb{A}_{M,L}^T \mathbb{A}_{M,L}$  and  $\mathbb{A}_{M,L}$  are identical, so it suffices to solve  $\mathbb{A}_{M,L} \mathbf{c} = \mathbf{0}$ , excluding the trivial solution  $\mathbf{c} = \mathbf{0}$  due to normalization.

REMARK 1. *Estimating the right-hand side of a  $dN$ -dimensional ODE system is challenging. For instance, estimating a generic cubic polynomial  $\phi$  defined on  $\mathbb{R}^{Nd}$  requires a polynomial basis of dimension  $\mathcal{O}((Nd)^3)$ , which grows exponentially with  $N$  and  $d$ , necessitating large datasets. In contrast, our problem is feasible with limited data due to the 1D nature of  $\phi$ , which reduces complexity. Furthermore,  $\phi$  couples the entire equation, leveraging the system's structure to constrain and regularize the estimation, enabling possible accurate recovery.*

*Identifiability.* Next, we examine conditions under which the true coefficients can be recovered. The matrix  $\mathbb{A}_{M,L}$  is inherently random due to stochastic initial conditions. Using a statistical inverse problem framework, we analyze identifiability as the number of trials  $M$  tends to infinity while  $L$  remains fixed.

PROPOSITION 2.2. *Assuming the initial conditions  $\mathbf{x}_1(0), \dots, \mathbf{x}_N(0)$  are i.i.d. samples from a probability distribution  $\mu_0$ , we have:*

$$(2.6) \quad \lim_{M \rightarrow \infty} \frac{1}{NML} \mathbb{A}_{M,L}^T \mathbb{A}_{M,L} = \mathbb{B} \in \mathbb{R}^{K \times K},$$

where

$$\mathbb{B}_{kk'} = \frac{1}{LN} \sum_{\ell=1}^L \mathbb{E}_{\mu_0} \left[ \sum_{i=1}^N \sum_{j=1}^N \sum_{j'=1}^N \xi_k(\|\mathbf{r}_{ij}(t_\ell)\|) \xi_{k'}(\|\mathbf{r}_{ij'}(t_\ell)\|) \langle \dot{\mathbf{x}}_i(t_\ell) - \mathbf{r}_{ij}(t_\ell), \dot{\mathbf{x}}_i(t_\ell) - \mathbf{r}_{ij'}(t_\ell) \rangle \right].$$

If  $\text{rank}(\mathbb{B}) = K - 1$ , the true coefficients can be identified up to a scaling factor.

There are several implications from this proposition. First, one needs to construct the basis on the support of the measure

$$\rho(dr) = \frac{1}{L} \sum_{l=1}^L \mathbb{E}_{\mu_0} \left[ \frac{1}{N^2} \sum_{i,i'=1}^{N,N} \delta_{\|\mathbf{x}_{i'}(t_l) - \mathbf{x}_i(t_l)\|}(dr) \right],$$

which describes the pairwise distances explored by the dynamical systems during the observation period. If a basis function  $\xi_k$  is supported outside  $\text{supp}(\rho)$ , it will yield a zero column in  $\mathbb{B}$ , leading to rank deficiency.

Second, the rank constraint on  $\mathbb{B}$  implies that it has a one-dimensional null space, and its second smallest singular value is positive. By applying classical random matrix theory, the second smallest singular value of  $\frac{1}{NML} \mathbb{A}_{M,L}^T \mathbb{A}_{M,L}$  converges to that of  $\mathbb{B}$ . This ensures the identifiability of  $\mathbf{c}^{\text{true}}$  when  $M$  is sufficiently large. The coefficients can then be estimated using the SVD algorithm by identifying the singular vector corresponding to the smallest singular value.

A special case arises when  $\phi$  is *1-sparse* in the basis representation, meaning only one of the coefficient entries is nonzero. In this scenario, the identifiability condition requires that exactly one column of  $\mathbb{B}$  is zero, while the remaining  $K - 1$  columns are linearly independent.

In our numerical experiments, we also explore the use of piecewise constant basis functions to approximate a continuous kernel function  $\phi$ . In this case,  $\phi$  does not lie in the span of the basis, and we instead find the eigenvector of  $\mathbb{B}$  corresponding to the minimal eigenvalue. We remark that such a matrix  $\mathbb{B}$  is a perturbation of the matrix constructed using a piecewise basis of the form  $\phi(\cdot) \chi_{I_i}(\cdot)$  on each subinterval  $I_i$ , up to a similarity transformation. The spectral gap of the gram matrix determines the robustness of eigenvector recovery, as governed by the Davis-Kahan theorem. Later, we demonstrate through numerical examples that in the case of small noise, one can achieve good recovery accuracy.

**3. Algorithm.** Building on the previous section, the estimation problem reduces to solving the homogeneous system:

$$(3.1) \quad \mathbb{A} \mathbf{c} = 0,$$

where, for brevity, we omit the indices  $M, L$ . To avoid the trivial solution  $\mathbf{c} = 0$ , a standard approach from prior works [44] is to fix one coefficient of  $\mathbf{c}$  to a nonzero value. Specifically, we set  $\mathbf{c}_{k^*} = 1$  for some  $k^* \in \{1, \dots, K\}$ , leading to the reformulated system:

$$(3.2) \quad \mathbb{A}_{-k^*} \mathbf{c}_{-k^*} = -\mathbb{A}_{k^*},$$

where  $\mathbb{A}_{k^*}$  denotes the  $k^*$ -th column of  $\mathbb{A}$ , and  $\mathbb{A}_{-k^*}$  is the matrix obtained by removing this column. This choice guarantees a nontrivial solution by ensuring at least one nonzero coefficient.

This approach is well justified because the estimation problem depends only on the relative magnitudes of the coefficients. Specifically, the dynamics of each  $\mathbf{x}_i$  are governed by the ratio:

$$(3.3) \quad \frac{\phi(|\mathbf{x}_{i'} - \mathbf{x}_i|)}{\sum_{j \in \mathcal{N}_i} \phi(|\mathbf{x}_j - \mathbf{x}_i|)},$$

which remains unchanged under normalization. Consequently, setting

$$(3.4) \quad \bar{\mathbf{c}} = \left( \frac{c_1}{c_{k^*}}, \dots, 1, \dots, \frac{c_K}{c_{k^*}} \right)$$

yields an equivalent solution, provided that  $\mathbf{c}_{k^*} \neq 0$ . Thus, the coefficients can be rewritten as:

$$(3.5) \quad \bar{\mathbf{c}} = \mathbf{e}_{k^*} + \hat{\mathbf{c}}_{-k^*},$$

where  $\mathbf{e}_{k^*}$  is the canonical basis vector in  $\mathbb{R}^K$ , and  $\hat{\mathbf{c}}_{-k^*}$  is the coefficient estimate from (3.2), embedded in  $\mathbb{R}^K$  with its  $k^*$ -th entry set to zero.

In summary, the estimation procedure consists of two key steps:

- Step 1: solving the reformulated system (3.2) for each  $k = 1, \dots, K$  using an appropriate optimization method, such as least squares.
- Step 2: model selection. Identifying the optimal index  $k^*$  to balance numerical stability and robustness.

**3.1. Challenges in Estimation.** Despite its conceptual simplicity, this approach faces several fundamental challenges:

**Essential ill-posedness.** The estimation problem could become inherently ill-posed when the dimension of the null space of  $\mathbb{B}$ —the expectation of the empirical matrix  $\mathbb{A}^T \mathbb{A}$ —exceeds one, i.e., when  $\text{rank}(\mathbb{B}) < K - 1$ . This could be caused by the nature of the dynamical systems, or by choosing basis functions outside of support of  $\rho$ . In such cases, even with an appropriate choice of  $k^*$ , solving (3.2) remains ill-posed, necessitating additional constraints or regularization to restore identifiability.

**Scarce and noisy data.** In practical applications, data is often limited ( $M$  is small) and subject to measurement noise. Let  $\tilde{\mathbf{x}}_i(t_l)$  and  $\tilde{\dot{\mathbf{x}}}_i(t_l)$  denote the noisy observations of position and velocity, respectively. The  $(i, k)$  entry of the empirical matrix  $\mathbf{A}^{(m,l)}$  in (2.5) is then perturbed as follows:

$$\begin{aligned} \tilde{\mathbf{A}}_{ik}^{(m,l)} &= \sum_{j \in \mathcal{N}_i} \xi_k \left( |\tilde{\mathbf{x}}_j^{(m)}(t_l) - \tilde{\mathbf{x}}_i^{(m)}(t_l)| \right) \left( \tilde{\dot{\mathbf{x}}}_i^{(m)}(t_l) - (\tilde{\mathbf{x}}_i^{(m)}(t_l) - \tilde{\mathbf{x}}_j^{(m)}(t_l)) \right) \\ &= \mathbf{A}_{ik}^{(m,l)} + \tilde{\epsilon}_{ik}^{(m,l)}, \end{aligned}$$

where  $\tilde{\epsilon}_{ik}^{(m,l)}$  represents the noise-induced perturbation. Consequently, the true system of equations is perturbed to:

$$(3.6) \quad \tilde{\mathbb{A}}_{M,L} \mathbf{c} = 0,$$

whereas the correct system should be:

$$(3.7) \quad \tilde{\mathbb{A}}_{M,L} \mathbf{c} = \eta_{M,L}, \quad \text{where} \quad \eta_{M,L} := \tilde{\epsilon}_{M,L} \mathbf{c}.$$

Here,  $\eta_{M,L}$  represents an unknown noise vector, making direct calibration of (3.6) infeasible. Furthermore, the right singular vectors of  $\tilde{\mathbb{A}}_{M,L}$  may deviate significantly from those of the true matrix  $\mathbb{A}_{M,L}$  (and thus  $\mathbb{B}$ ), complicating the identification of the correct null space. This sensitivity to noise underscores the need for robust estimation techniques, such as regularization or noise-aware optimization strategies.

Finally, the estimation performance in step 1 would affect the model selection performance in step 2.

**3.2. A Sparse Bayesian Learning (SBL) Approach.** For clarity, we consider a universal form of (3.7) in linear inverse problem as:

$$(3.8) \quad \mathbf{b} = \Phi \mathbf{w} + \boldsymbol{\eta},$$

where  $\mathbf{b} = -\tilde{\mathbf{A}}_{k*} \in \mathbb{R}^{dNML}$  is a vector of indirect measurements/observations,  $\mathbf{w} = \mathbf{c}_{-k*} \in \mathbb{R}^{K-1}$  is the vector of unknowns which we seek to recover,  $\Phi = \tilde{\mathbf{A}}_{-k*} \in \mathbb{R}^{dNML \times (K-1)}$  is a known linear forward operator, and  $\boldsymbol{\eta}$  represents an unknown noise vector. We employ the *Sparse Bayesian Learning (SBL)* framework [44], a principled and flexible framework that address the challenges in section 3.1.

SBL is particularly suited for high-dimensional, noisy data, leveraging probabilistic inference and adaptive regularization to mitigate ill-posedness. Unlike conventional methods requiring manual tuning, SBL infers regularization parameters directly from data, improving efficiency and stability. Beyond regularization, SBL naturally quantifies uncertainty, accounting for variability due to initial conditions and measurement noise. This facilitates principled model selection and provides confidence measures for inferred parameters.

**3.2.1. Data and Observation Models.** To begin with, we model the trajectory data  $\boldsymbol{\eta}$  by conditioning on observations and incorporating an observational noise model. The dataset is defined as:

$$(3.9) \quad \tilde{\mathcal{D}}_{M,L} = \{\mathbf{X}^{(m)}(t_l), \dot{\mathbf{X}}^{(m)}(t_l) + \boldsymbol{\zeta}^{(m,l)}\}_{m,l=1}^{M,L},$$

where  $\boldsymbol{\zeta}^{(m,l)} = \{\boldsymbol{\zeta}_i^{(m,l)}\}_{i=1}^N$  are i.i.d. random variables sampled from  $\mathcal{N}(\mathbf{0}, \sigma_{\text{velocity}}^2 I_{dN})$ . This setup leads to a distribution for  $\tilde{\boldsymbol{\epsilon}}_{ik}^{(m,l)}$ :

$$\tilde{\boldsymbol{\epsilon}}_{ik}^{(m,l)} \sim \mathcal{N}\left(\mathbf{0}, \sigma_{\text{velocity}}^2 \sum_{j \in \mathcal{N}_i} \xi_k^2 (|\mathbf{x}_j^{(m)} - \mathbf{x}_i^{(m)}|)\right).$$

The observation noise  $\boldsymbol{\eta}^{(m,l)} \in \mathbb{R}^{Nd}$  is then modeled as:

$$(3.10) \quad \boldsymbol{\eta}^{(m,l)} \sim \mathcal{N}\left(\mathbf{0}, \text{diag}\left(\sum_{j \in \mathcal{N}_i} \sigma_{\text{velocity}}^2 c_k^2 \xi_k^2 (|\mathbf{x}_j^{(m)} - \mathbf{x}_i^{(m)}|)\right)\right).$$

Therefore, the realizations of each random variable in (3.8) respectively are the observable data  $\mathbf{b}$  and noise vector  $\boldsymbol{\eta}$ , and a hierarchical Bayesian model based on Bayes' theorem then provides an estimate of the full posterior distribution of  $\mathbf{w}$  given by

$$(3.11) \quad p(\mathbf{w}, \boldsymbol{\Theta} | \mathbf{b}) \propto p(\mathbf{b} | \mathbf{w}, \boldsymbol{\Theta}) p(\mathbf{w} | \boldsymbol{\Theta}) p(\boldsymbol{\Theta})$$

where  $\boldsymbol{\Theta}$  are all the involved parameters in the random variables, where  $p(\mathbf{b} | \mathbf{w}, \boldsymbol{\Theta})$  is the likelihood density function determined by the relationship between  $\mathbf{b}$  and  $\mathbf{w}$ , and assumptions on  $\boldsymbol{\eta}$ ,  $p(\mathbf{w} | \boldsymbol{\Theta})$  is the density of the prior distribution encoding a priori assumptions about the weights  $\mathbf{w}$ , and  $p(\boldsymbol{\Theta})$  is the hyperprior density for all other involved parameters.

**3.2.2. The Likelihood.** The likelihood function  $p(\mathbf{b} | \mathbf{w}, \boldsymbol{\Theta})$  models the connection between the weights  $\mathbf{w}$ , the indirect measurements  $\mathbf{b}$ , and the noise vector  $\boldsymbol{\eta}$ . Based on the derivation in (3.10), for simplicity, we can assume that  $\boldsymbol{\eta}$  follows a zero-mean Gaussian distribution with diagonal identical covariance:

$$\boldsymbol{\eta} \sim \mathcal{N}(\mathbf{0}, \sigma_{\text{noise}}^2 I_{dNML}),$$

where  $\sigma_{\text{noise}}^2$  will be estimated from the data. Then, the likelihood is given by

$$(3.12) \quad p(\mathbf{b} | \mathbf{w}, \sigma_{\text{noise}}^2) = (2\pi)^{-dNLM/2} \sigma_{\text{noise}}^{-dNLM} \exp\left\{-\frac{\|\mathbf{b} - \Phi \mathbf{w}\|^2}{2\sigma_{\text{noise}}^2}\right\}.$$

**REMARK 2.** The likelihood function given by (3.12) is a classical assumption for SBL that was considered, for instance, in [44]. More precisely, based on (3.10), we can also restrict  $\boldsymbol{\eta}$  to be independent but not necessarily identically distributed, i.e.,  $\boldsymbol{\eta} \sim \mathcal{N}(\mathbf{0}, \Sigma)$  for some block diagonal positive definite matrix  $\Sigma$  [50]. In practice, since  $\boldsymbol{\eta}$  is a weighted average of  $\tilde{\boldsymbol{\epsilon}}$ , the numerical results show that we can still find good estimates of  $\mathbf{w}$  under the identical assumption.

**3.2.3. The Sparse Prior and Hyperprior.** Direct application of maximum likelihood estimation for  $\mathbf{w}$  and  $\sigma_{\text{noise}}^2$  from (3.12) would usually lead to severe overfitting. To address this issue and seek the sparse solution, sparse Bayesian learning ‘constrains’ the targeted parameters  $\mathbf{w}$  by introducing an explicit sparse prior probability distribution  $p(\mathbf{w}|\Theta)$ . There are a variety of sparsity-promoting priors to choose from, including but not limited to TV-priors, Laplace priors, and hyper-Laplacian distributions based on  $l^p$ -quasinorms with  $0 < p < 1$  [2, 24, 41].

In our paper, we consider the commonly used prior, the Gaussian prior, where

$$(3.13) \quad p(\mathbf{w}|\Theta) = \prod_{k=1}^K p(w_k|\gamma_k) \quad \text{and} \quad p(w_k|\gamma_k) = \mathcal{N}(0, \gamma_k^{-1}),$$

with some hyperparameters  $\gamma = (\gamma_1, \dots, \gamma_K)$ . Note that  $\gamma_k$  must be allowed to have distinctly different values for the conditionally Gaussian prior to promote sparsity, and this can be achieved by treating  $\gamma$  as random variables with uninformative hyperprior  $p(\gamma)$ , like a uniform hyperpriors (over a logarithmic scale). Since all scales are equally likely, a pleasing consequence of the use of such ‘improper’ hyperpriors here is that of scale-invariance [44].

REMARK 3. *It has been shown that the sparse Bayesian learning method is equivalent to an iterative reweighted  $L_1$  method, which is more efficient to find the maximally sparse representations compared with the regular  $L_1$  regularized least square methods [48].*

In our paper, we consider both flat hyperprior and another hyperprior which enhances the knowledge of sparsity in our experiments. We employ a hierarchical Laplace hyperprior as proposed in [3], which is constructed in two stages with hyperparameters  $(\gamma, \lambda)$ :

- **Stage 1:** Each  $\gamma_k$  follows a gamma distribution, which promotes sparsity:

$$(3.14) \quad p(\gamma_k|\lambda) = \Gamma(\gamma_k|1, \lambda/2).$$

- **Stage 2:** The hyperparameter  $\lambda$  is modeled using a non-informative Jeffrey’s prior:

$$(3.15) \quad p(\lambda) \propto \frac{1}{\lambda}.$$

REMARK 4. *The  $L_1$  regularization formulation is equivalent to using a direct Laplace prior on the coefficients  $\mathbf{w}$ , i.e.,  $p(\mathbf{w}|\lambda) = \frac{\lambda}{2} \exp(-\lambda|\mathbf{w}|)$  [3]. However, this formulation of the Laplace prior does not allow for a tractable Bayesian analysis, since it is not conjugate to the likelihood. To alleviate this, the hierarchical priors are employed.*

REMARK 5. *A common choice of informative hyperprior is the gamma distribution since it is a conjugate for the conditionally Gaussian distributions. However, compared with the Gaussian prior, the Laplace prior enforces sparsity more strongly by concentrating the posterior mass along the axes, favoring solutions with many coefficients close to zero. Additionally, the Laplace prior is log-concave, which ensures unimodal posterior distributions and eliminates local minima, simplifying the optimization process [3].*

### 3.2.4. Bayesian Inference.

*Posterior of  $\mathbf{w}$  given  $\Theta$ .* Combining the likelihood and prior using Bayes’ rule, the posterior distribution of all the unknowns  $(\mathbf{w}, \Theta)$  with data  $\mathbf{b}$  is given by:

$$(3.16) \quad p(\mathbf{w}, \Theta|\mathbf{b}) = \frac{p(\mathbf{b}|\mathbf{w}, \Theta)p(\mathbf{w}, \Theta)}{p(\mathbf{b})}.$$

Since the marginal likelihood  $p(\mathbf{b})$  is intractable, we decompose the posterior as:

$$(3.17) \quad p(\mathbf{w}, \Theta|\mathbf{b}) = p(\mathbf{w}|\mathbf{b}, \Theta)p(\Theta|\mathbf{b}).$$

Therefore, given  $\Theta$ , the first term, i.e., the posterior distribution of  $\mathbf{w}$  given data,  $p(\mathbf{w}|\mathbf{b}, \Theta)$ , is Gaussian and can be computed analytically:

$$(3.18) \quad p(\mathbf{w}|\mathbf{b}, \Theta) = \mathcal{N}(\boldsymbol{\mu}, \boldsymbol{\Sigma}),$$

where

$$(3.19) \quad \boldsymbol{\Sigma} = (\text{diag}(\gamma) + \sigma_{\text{noise}}^{-2} \boldsymbol{\Phi}^T \boldsymbol{\Phi})^{-1}, \quad \boldsymbol{\mu} = \sigma_{\text{noise}}^{-2} \boldsymbol{\Sigma} \boldsymbol{\Phi}^T \mathbf{b}.$$

*Optimization of hyperparameters  $\Theta$ .* For the second term, instead of applying Bayesian inference over those hyperparameters  $\Theta$  (which is analytically intractable), sparse Bayesian learning is formulated as a type-II maximum likelihood procedure, i.e., the (local) maximisation with respect to  $\Theta$  of the marginal likelihood  $p(\mathbf{b}, \Theta)$ , or equivalently its logarithm  $\mathcal{L}(\Theta)$ ,

$$(3.20) \quad \mathcal{L}(\Theta) = \log p(\mathbf{b}, \Theta) = \log \int p(\mathbf{b}|\mathbf{w}, \Theta)p(\mathbf{w}|\Theta) d\mathbf{w}.$$

Once a most-probable values  $\Theta_{MP}$  have been found, in practice they can be plugged into (3.19) to give a posterior mean (most probable point estimate for the parameters,  $\hat{\mathbf{w}}_{MP} = \boldsymbol{\mu}_{MP}$ ).

Empirically, the local maximisation of the marginal likelihood  $p(\mathbf{b}, \Theta)$  with respect to  $\Theta$  has been seen to work highly effectively with the greedy algorithm which select a candidate  $\gamma_k$  at each iteration and update  $\gamma_k$  by maximizing  $\mathcal{L}(\Theta)$  when all components of  $\boldsymbol{\gamma}$  except  $\gamma_k$  are kept fixed. For the flat hyperprior, we adopt the algorithm proposed in [45], and for the hierarchical Laplacian hyperprior, we adopt the algorithm proposed in [3].

The optimal values of many of the hyperparameters  $\gamma_k$  would be infinite [44], which leads to a posterior with many weights  $w_k$  infinitely peaked at zero and results in the sparsity of the model.

Finally, for the noise variance  $\sigma_{\text{noise}}^2$ , differentiation of (3.12) leads to the re-estimate:

$$(3.21) \quad \hat{\sigma}_{\text{noise}}^2 = \frac{\|\mathbf{b} - \Phi\hat{\mathbf{w}}\|}{dNML - \sum_k \gamma_k}$$

**REMARK 6.** A Gamma prior can be placed on  $\sigma_{\text{noise}}^2$  to estimate it in the Bayesian framework. Unfortunately, this method cannot be used in practice with the greedy algorithms since the reconstruction and, therefore, the estimation of  $\sigma_{\text{noise}}^2$  using this method are unreliable at early iterations. Due to the under-determined nature of the compressive sensing problem, once the estimate of  $\sigma_{\text{noise}}^2$  is very far from its true value, the reconstruction quality is also significantly affected. Therefore, we fix the estimate of this parameter in the beginning of the algorithm using  $\sigma_{\text{noise}}^2 = 0.01\|\mathbf{b}\|_2^2$  inspired by [3].

**3.3. Model Selection.** In general, the true basis function  $\xi_{k^*}$  in the representation of  $\phi$  is unknown. To address this, we test each candidate function  $\xi_{k^*}$  for  $k^* \in \{1, \dots, K\}$  until a model in (3.2) yields a sparse and accurate solution. When the candidate function  $\xi_{k^*}$  is not part of the true representation, the resulting coefficient vector  $\mathbf{w}$  will lack sparsity, and the prediction error will be large. Conversely, when the correct candidate is selected, the coefficient vector  $\mathbf{w}$  will be sparse, and the prediction error will be small. This approach provides a clear indicator of when the correct model has been identified. Although redundant information arises—since each term in the correct model can be used as a candidate function on the left-hand side, and the resulting models can be cross-referenced—this process is highly parallelizable, allowing each candidate term to be tested simultaneously.

In practice, one may randomly select several (or all) candidate indices  $k$  and choose the one with the smallest error according to a pre-selected error measure as  $k^*$ . Several valid measures for model selection are discussed in [19, 49], e.g., the weighted predictive error,

$$(3.22) \quad \text{wPE} = \frac{\|\Phi\mathbf{w} - \Phi\hat{\mathbf{w}}\|_2^2}{\|\hat{\mathbf{w}}\|_2^2},$$

which evaluates the model fit, or the weighted estimation uncertainty,

$$(3.23) \quad \text{wEU} = \frac{\text{tr}(\hat{\boldsymbol{\Sigma}}^{(k^*)})}{\|\hat{\boldsymbol{\mu}}^{(k^*)}\|_2^2},$$

which measures the relative uncertainty of the estimated coefficients. In this work, we propose a new criteria to select  $k^*$  as the candidate that minimizes the weighted total uncertainty (wTU) constructed by

$$(3.24) \quad \text{wTU} = \frac{\hat{\sigma}_{\text{noise}}^2 + \text{tr}(\hat{\boldsymbol{\Sigma}}^{(k^*)})}{1 + \|\hat{\boldsymbol{\mu}}^{(k^*)}\|_2^2},$$

which include both uncertainties of the estimated coefficients by the variances,  $\text{tr}(\hat{\Sigma}^{(k^*)})$ , and the model itself by the predicted error,  $\sigma_{\text{noise}}^2$ . We normalize the total uncertainty by the norm of the coefficients to compare them with different selections of  $k^*$ .

This structured approach leverages advanced statistical techniques to address the challenges of noisy, high-dimensional data, ensuring that the resulting model is both sparse and accurate. The numerical results show that this weighted total uncertainty can correctly select the  $k^*$  in our examples. The entire procedure is summarized in Algorithm 3.1, and the desire estimation of  $\hat{c}_{-k^*}$  is given by  $\hat{\mu}^{(k^*)}$  using (3.19).

---

**Algorithm 3.1 Learning kernels**


---

**Input:**  $\tilde{D}_{M,L} = \{\tilde{X}^{(m)}(t_l), \tilde{X}^{(m)}(t_l)\}_{M,L}$  (training data),  $\mathcal{S} = \{\xi_k\}_{k=1}^K$  (basis-functions)

- 1: compute  $\tilde{\mathbb{A}} = (\tilde{\mathbf{A}}^{(1,1)}, \dots, \tilde{\mathbf{A}}^{(M,L)})^T \in \mathbb{R}^{dNLM \times K}$  using (2.5);
- 2: **for**  $k^* = 1$  to  $K$  **do**
- 3:   Calculate the posterior distribution  $p(\mathbf{w}_k | \tilde{\mathbb{A}}_k)$  with  $\tilde{\mathbb{A}}_k = -\tilde{\mathbb{A}}_{-k} \mathbf{w}_k$  using the fast greedy algorithm, let the estimated posterior mean be  $\hat{\mu}^{(k^*)}$ , the variance be  $\hat{\Sigma}^{(k^*)}$ ;
- 4:   Re-estimate the noise variance  $\sigma_{\text{noise}}^2$  using (3.21);
- 5: **end for**
- 6: pick  $k^*$  with the smallest weighted total uncertainty defined by (3.24);
- 7:  $\bar{\phi}^* = \xi_{k^*} + \mu^{(k^*)} \cdot \xi_{-k^*}$ ;

**Output:**  $\bar{\phi}^*$

---

Note that the computational complexity for ensemble the matrix  $\tilde{\mathbb{A}}$  is  $\mathcal{O}(dN^2MLK)$ , and for each iteration in the model selection procedure, the computational complexity is approximately  $\mathcal{O}((dNML)^3K)$  since it involves computing an inversion of a matrix with dimension  $dNML * dNML$  while evaluating  $\mathcal{L}(\theta)$  and we assume  $K \ll dNML$ . However, in practice, we can reduce this order since the matrix is often very sparse, as shown in our numerical experiments.

**REMARK 7.** *Since one of the main goals of our strategy is to avoid the trivial solution/estimation, and for  $\mathbb{A}_{k^*} \approx 0$  (equals zero at most entries), it implies that the  $c_{k^*} = 0$  or we do not have enough information to learn the right coefficient of  $\xi_k$  with the given observational data. Therefore, in our numerical examples, we exclude the candidate  $k^*$  if more than half of the entries of  $\mathbb{A}_{k^*}$  are zero. This can not only accelerate the model selection process, but also exclude the misspecification caused by inadequate information.*

**3.4. Uncertainty Quantification.** The posterior variance  $\Sigma^{(k^*)}$  can be used as a good indicator for the uncertainty of the estimation for  $\hat{c}_{-k^*}$  based on our Bayesian approach. Therefore, for the estimation of  $\phi$ , we can construct an uncertainty quantification region for any  $r \in \mathbb{R}^+$  by:

$$\begin{aligned}
 \xi_{k^*}(r) + \sum_{k \neq k^*} \min\{(\mu_k^{(k^*)} - 2\Sigma_{kk}^{(k^*)})\xi_k(r), (\mu_k^{(k^*)} + 2\Sigma_{kk}^{(k^*)})\xi_k(r)\} &\leq \bar{\phi}^* \\
 (3.25) \quad &\leq \xi_{k^*}(r) + \sum_{k \neq k^*} \max\{(\mu_k^{(k^*)} - 2\Sigma_{kk}^{(k^*)})\xi_k(r), (\mu_k^{(k^*)} + 2\Sigma_{kk}^{(k^*)})\xi_k(r)\}.
 \end{aligned}$$

where the mean  $\mu^{(k^*)}$  and the covariance matrix  $\Sigma^{(k^*)}$  are again given by (3.19) with the estimated  $\gamma$  and  $\sigma_{\text{noise}}^2$ .

#### 4. Numerical Experiments.

*Numerical setup.* We consider a system of  $N$  interacting agents, where each agent's state vector lies in  $\mathbb{R}^d$ . We simulate agent trajectories over the time interval  $[0, T]$ , with parameters specified in Tables 1, 3, and with i.i.d. initial conditions sampled from a prescribed uniform distribution. For training data, we generate  $M$  independent trajectories, each observed at  $L$  equidistant time points  $0 = t_1 < t_2 < \dots < t_L = T$ . Additive i.i.d. Gaussian noise is applied to the agent velocities,  $\dot{\mathbf{X}}^{(m)}(t_l)$ , as specified in (3.9) with different noise levels w.r.t. the average velocity, i.e. the standard deviation of the noise equals to the percentages

(0%, 5%, 10%, ...) of the mean

$$\bar{v} = \frac{1}{NML} \sum_{i,m,l=1}^{N,M,L} \dot{\mathbf{x}}_i^{(m)}(t_l).$$

And the empirical distribution of the pairwise distance, denoted  $\rho_r$ , is computed by the pairwise distance in each training dataset respectively,

$$\rho_r^{\mathcal{D}_{M,L}}(dr) = \frac{1}{ML} \sum_{m,l=1}^{M,L} \frac{1}{N(N-1)} \sum_{i=1}^N \sum_{i' \in \mathcal{N}_i} \delta_{\|\mathbf{x}_{i'}^{(m)}(t_l) - \mathbf{x}_i^{(m)}(t_l)\|}(dr),$$

where  $\delta$  is the Dirac distribution. Since the learned interaction kernel  $\hat{\phi}$  may differ from the ground truth  $\phi_{true}$  by a multiplicative constant, we normalize all estimations using a relative  $L_1$ -norm weighted by the empirical distribution  $\rho_r$ :

$$\frac{\int |\phi_{true}(r)| d\rho_r}{\int |\hat{\phi}(r)| d\rho_r}.$$

This normalization enables consistent comparison across noise levels and data sizes. All ODE systems are numerically integrated using MATLAB<sup>®</sup> R2023a's ode15s solver, with relative and absolute tolerances set to  $10^{-5}$  and  $10^{-6}$  respectively.

**4.1. First-order systems: 1D and 2D opinion dynamics model.** Opinion dynamics models are widely used to understand collective behavior in social systems, including consensus formation, voting, and decentralized decision-making. We consider a first-order system of  $N$  interacting agents, where interactions are inherently nonsymmetric. The evolution of each agent's opinion is governed by the following first-order differential equation:

$$(4.1) \quad \dot{\mathbf{x}}_i = \sum_{i'=1}^N \frac{\phi(|\mathbf{x}_{i'} - \mathbf{x}_i|)}{\sum_{j \neq i}^N \phi(|\mathbf{x}_j - \mathbf{x}_i|)} (\mathbf{x}_{i'} - \mathbf{x}_i).$$

A widely used kernel in modeling opinion exchange involves employing a discontinuous interaction kernel. Such kernels effectively capture threshold-based interactions, where individuals adjust their opinions depending on the proximity of their current stance to others [36]. One example of such an interaction function is defined as:

$$(4.2) \quad \phi(r) = \begin{cases} 1 & \text{if } 0 \leq r < 0.5 \\ 0.1 & \text{if } 0.5 \leq r < 1 \\ 0 & \text{if } r \geq 1 \end{cases}$$

The interaction kernel  $\phi$  characterizes non-repulsive interactions among agents, ensuring that each individual seeks to align its opinion with those of its connected neighbors. This framework effectively encapsulates key aspects of opinion formation, where both close-range and long-range interactions contribute to the evolution of collective consensus.

$N$	$M$	$L$	$[0, T]$	Learning domain	$K$	$\xi_k(r)$
100	3	6	$[0, 5]$	$[0, 10]$	100	$\chi_{[\frac{10(k-1)}{K}, \frac{10k}{K}]}(r)$

Table 1: System and learning parameters for the first-order opinion dynamics model.

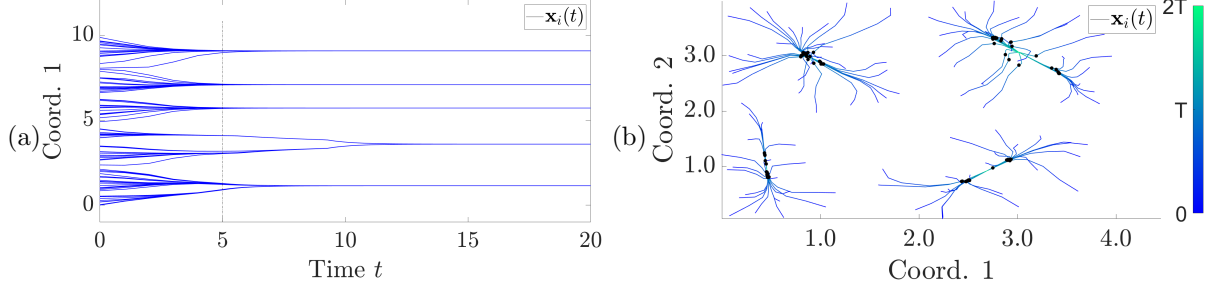


Fig. 1: Trajectory profiles for the opinion dynamics for 1D and 2D examples

We approximate the true interaction kernel using a piecewise constant expansion:

$$(4.3) \quad \phi = \sum_{k=1}^{100} c_k \xi_k,$$

where  $\xi_k = \chi_{[\frac{10(k-1)}{K}, \frac{10k}{K}]}(r)$  and the coefficients  $c_k$  are given by:

$$(4.4) \quad c_k = \begin{cases} 1 & \text{if } k = 1, \dots, 5 \\ 0.1 & \text{if } k = 6, \dots, 10 \\ 0 & \text{if } k = 11, \dots, 100 \end{cases}$$

This representation matches the ground truth kernel in (4.2) and enables exact recovery under ideal conditions.

Figure 2 demonstrates that in both 1D and 2D dynamics, our method can capture the exact function when the noise level is small. And when noise increases, although high noise affects the estimation accuracy near  $r = 0$ , where pairwise data is sparse, the model still captures critical structural features of  $\phi$  (e.g., discontinuities), ensuring accurate long-term trajectory prediction.

The predictive error of  $\phi$  in the relative  $L_\infty$ -norm with different training data sizes varied by  $M$  is shown in Figure 3. When the noise level is small, our method can precisely estimate  $\phi$  with only small amount of observations. And when the noise level is large, increasing the number of observations would reduce the predictive error in  $\phi$  as we expected.

We also evaluate model selection performance using three criteria: wTU in (3.24) (our proposed thresholded utility loss), wPE in (3.22) (predictive error), and wEU in (3.23) (estimation uncertainty). Table 2 summarizes the average success rate for each criterion in identifying the correct support  $k^* \in \{1, \dots, 10\}$ . Notably, wTU consistently selects the correct model across all noise levels, while the other two criteria fail under moderate to high noise, especially for wEU, which aligns with observations in [49], where small-magnitude coefficients dominate uncertainty estimates. Although we can add a threshold for the estimated coefficients to correct the model selection with wEU as suggested in [49], the wTU we proposed leverages thresholding over weighted test loss, offering more robustness without additional tuning.

Figure 4 shows the average running time for estimating  $\phi$  with the Laplace hyperprior given different sizes of datasets. The results are measured with 50 trials for different  $M$ , and each of them including 5 different levels of noise as we measure the prediction errors above. The shadow regions indicate the standard deviation of the running times, and the results show that when  $d = 1$ , the average running time is roughly controlled by  $\mathcal{O}(M^{3/2})$ , and  $\mathcal{O}(M^{5/2})$  for  $d = 2$ . As mentioned in section 3.3, the theoretical computational complexity is  $\mathcal{O}(M^3)$ , however, we can get lower complexity in practice because of the sparsity of our ensemble matrices.

**4.2. Second-order systems: Cucker-Smale models.** Our framework naturally extends to second-order systems such as the Cucker-Smale model, which describes the collective motion of interacting agents governed by second-order dynamics. Such models capture richer dynamics observed in physical and biological swarming systems, where alignment is velocity-driven. Consider the system of  $N$  agents evolving according

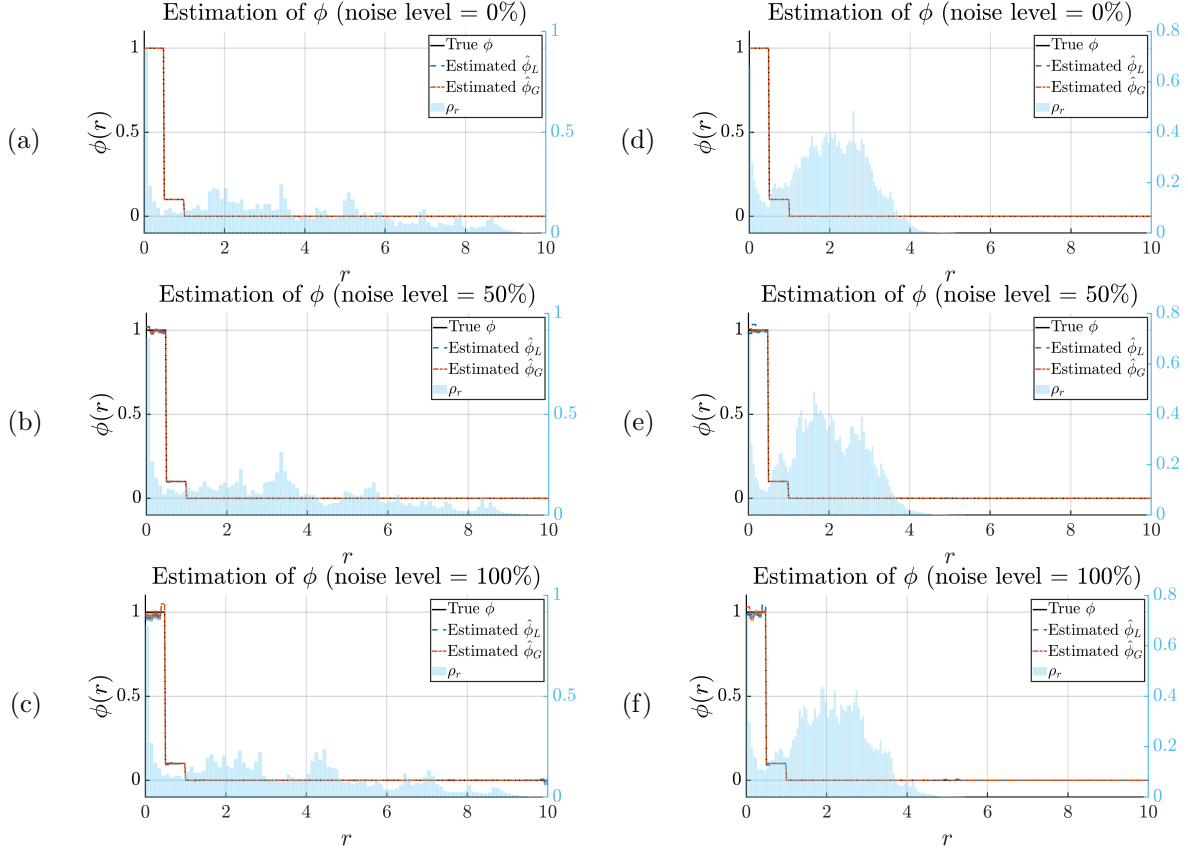


Fig. 2: Estimated interaction kernels  $\hat{\phi}$  for 1D (left) and 2D (right) opinion dynamics under increasing noise levels ( $(M, L) = (3, 6)$ ).

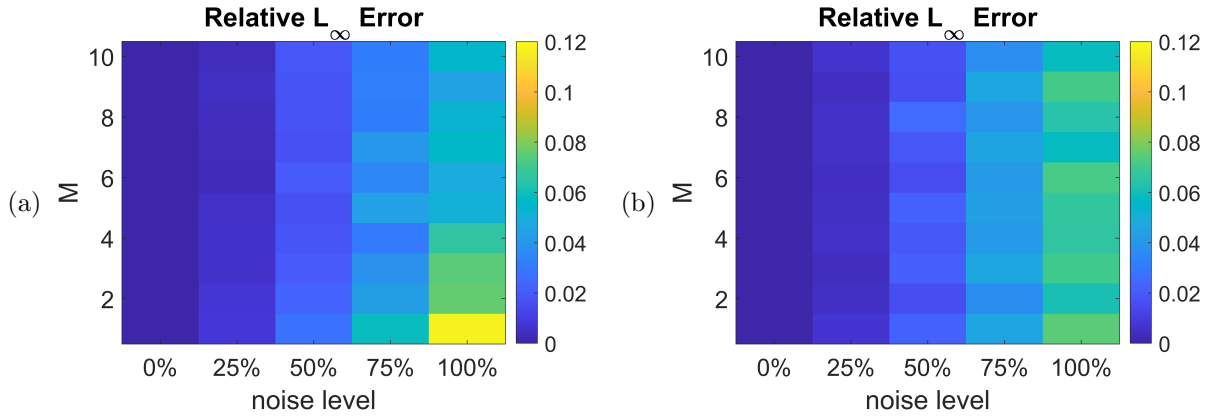


Fig. 3: Prediction error of  $\phi$  for (a) 1D and (b) 2D systems with different  $M$  and noise levels ( $L = 6$  fixed).

to the equation:

$$(4.5) \quad m_i \ddot{\mathbf{x}}_i = \sum_{i'=1}^N \frac{\phi(\|\mathbf{x}_{i'} - \mathbf{x}_i\|)}{\sum_{j=1}^N \phi(\|\mathbf{x}_j - \mathbf{x}_i\|)} (\dot{\mathbf{x}}_{i'} - \dot{\mathbf{x}}_i),$$

Table 2: The average successful rate of different model selection criteria.

$d = 1$	noise level				
Criterion	0%	25%	50%	75%	100%
wTU	1.00	1.00	1.00	1.00	1.00
wPE	1.00	1.00	1.00	0.98	0.98
wEU	1.00	0.04	0	0	0
$d = 2$	noise level				
Criterion	0%	25%	50%	75%	100%
wTU	1.00	1.00	1.00	1.00	1.00
wPE	1.00	1.00	1.00	0.99	0.99
wEU	1.00	0.11	0	0	0

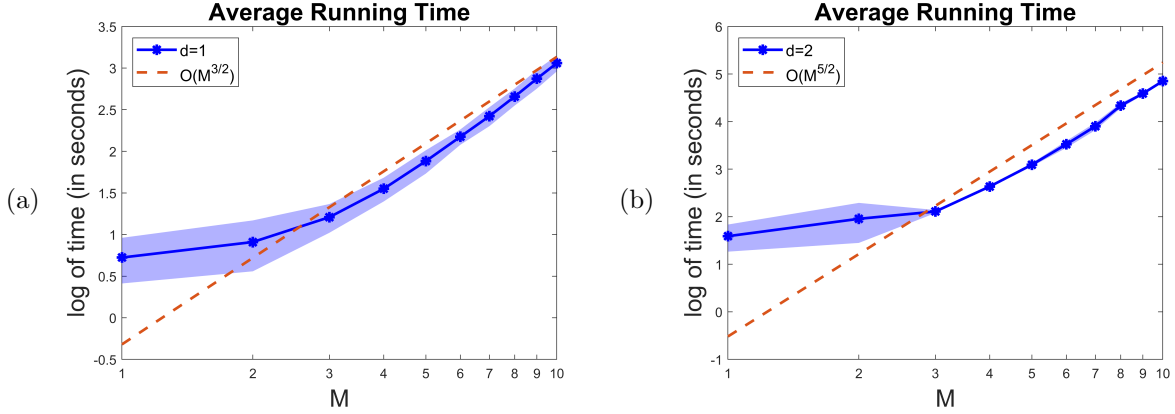


Fig. 4: Average running time for learning opinion dynamics models with two different dimensions.

where  $m_i$  denotes the mass of agent  $i$ , and  $\ddot{\mathbf{x}}_i$  represents its acceleration. This formulation captures how each agent's acceleration is influenced by the relative velocities of its neighbors, with interactions weighted by distance. Notably, this model is well-suited for systems with non-homogeneous phase spaces, as introduced in [34], where local interactions play a dominant role in shaping the global dynamics.

Our method can be adapted to infer the interaction dynamics in second-order systems with minor modifications. Based on (4.5), given training data  $\{\mathbf{X}^{(m,l)}, \dot{\mathbf{X}}^{(m,l)}, \ddot{\mathbf{X}}_{\sigma_2}^{(m,l)}\}$ , we define the regression matrix by isolating  $\phi(\|\mathbf{x}_j - \mathbf{x}_i\|)$  and projecting onto a set of basis functions  $\xi_k(r)$ , i.e., we construct the regression matrix  $\mathbf{A} = [\mathbf{A}_{ik}] \in \mathbb{R}^{2dN \times K}$  as follows:

$$(4.6) \quad \mathbf{A}_{ik} = \sum_{j \in \mathcal{N}_i} \xi_k(\|\mathbf{x}_j - \mathbf{x}_i\|) (m_i \ddot{\mathbf{x}}_i - (\dot{\mathbf{x}}_i - \dot{\mathbf{x}}_j)),$$

where  $\mathcal{N}_i$  denotes the neighborhood of agent  $i$ , and  $\xi_k(\|\mathbf{x}_j - \mathbf{x}_i\|)$  is a basis function that depends on the inter-agent distance.

To evaluate our framework, we consider two representative examples of second-order interaction dynamics using prototype kernels that model either multi-cluster or mono-cluster flocking behavior. Figure 5 depicts the resulting trajectory profiles.

We consider a system of dimension  $dN = 200$  and summarize the common system parameters in Table 3.

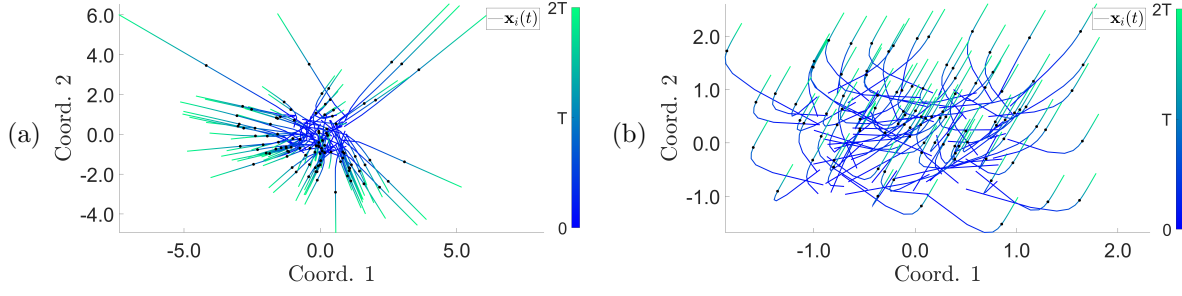


Fig. 5: Trajectory profiles for the Cucker-Smale system under different interaction kernels.

$m_i$	$N$	$d$	$M$	$L$	$[0, T; T_f]$	Learning domain	$K$	$\xi_k(r)$
1	100	2	5	6	$[0, 5; 10]$	$[0, 5]$	100	$\chi_{[\frac{10(k-1)}{K}, \frac{10k}{K}]}(r)$

Table 3: System and learning parameters for the Cucker-Smale model.

*Example 1 (Cut-off kernel at a finite distance).* In the first example, we use a compactly supported interaction kernel:

$$\phi(r) = \chi_{[0, 0.5]}(r),$$

which enforces interactions only between agents within a radius of 0.5. This leads to locally influenced multi-cluster flocking behavior, as shown in Figure 5(a). The corresponding estimation results using a piecewise constant basis are shown in Figure 6.

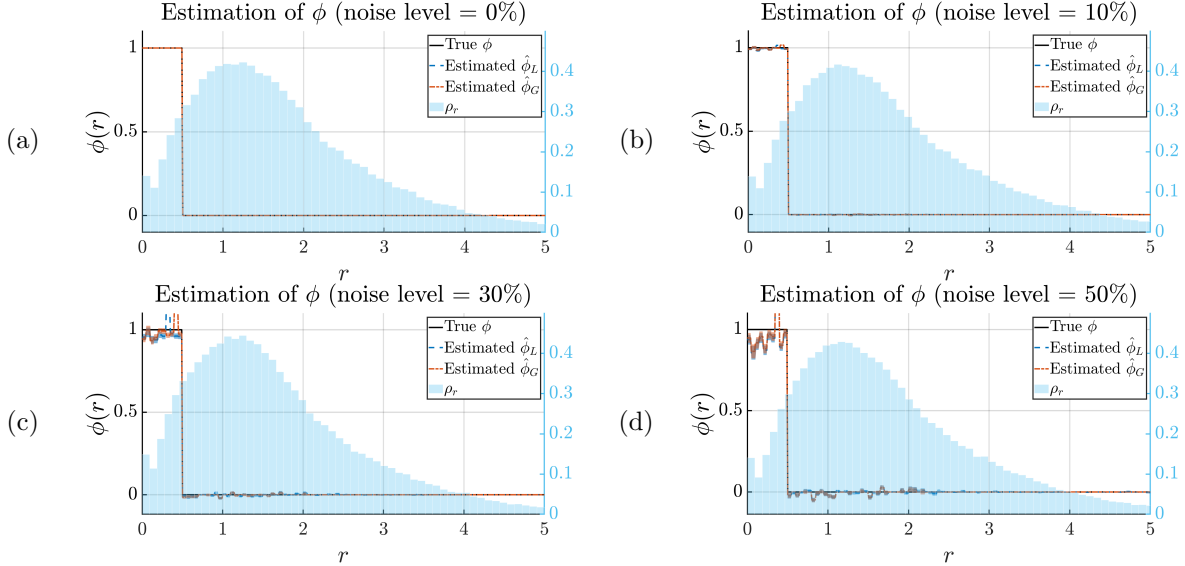


Fig. 6: Estimated interaction kernels  $\hat{\phi}$  for the compactly supported kernel case under increasing noise levels.

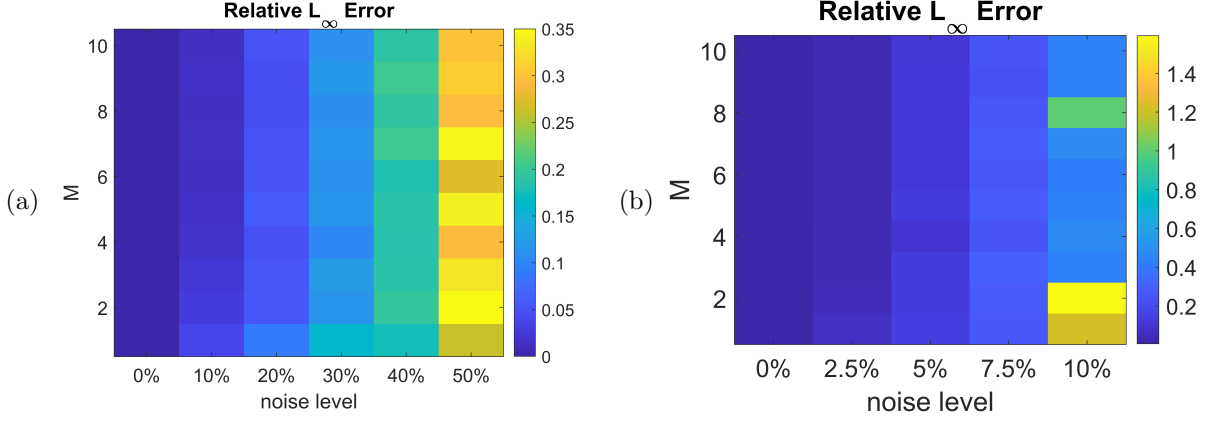


Fig. 7: Prediction error of  $\phi$  for Cucker-Smale model in (a) cut-off kernel, (b) rapid decay kernel, with different  $M$  and noise levels ( $L = 6$  fixed).

*Example 2 (Rapid decay kernel).* In the second example, we examine a smooth, rapidly decaying interaction kernel:

$$\phi(r) = \frac{1}{(1 + r^2)^{1/4}},$$

which maintains long-range influence while emphasizing nearby interactions. This kernel enables a balance between local coherence and global flocking. The true trajectories and resulting estimations are presented in Figures 5(b) and 8, respectively.

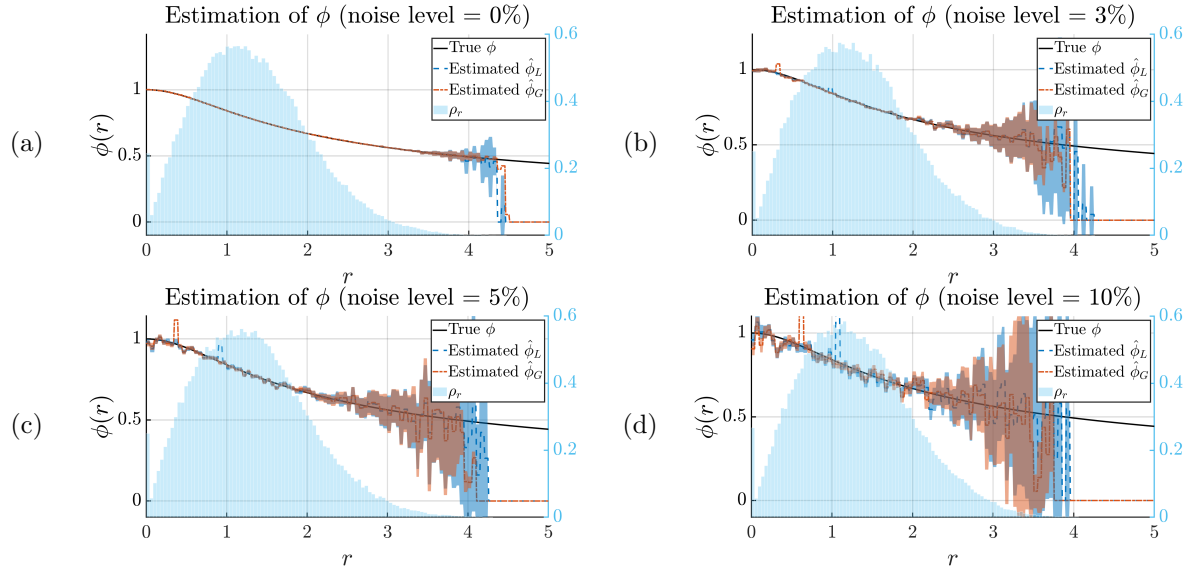


Fig. 8: Estimated interaction kernels  $\hat{\phi}$  for the rapidly decaying kernel under increasing noise levels.

As shown in Figures 8(c)–(d), high noise levels degrade the estimation quality, particularly in intervals with limited data support. This is expected, as we approximate a smooth kernel using piecewise constant basis functions. Nevertheless, Figure 9 demonstrates that despite local discrepancies in  $\hat{\phi}$ , the predicted trajectories remain accurate, highlighting the model's robustness in forward simulation.

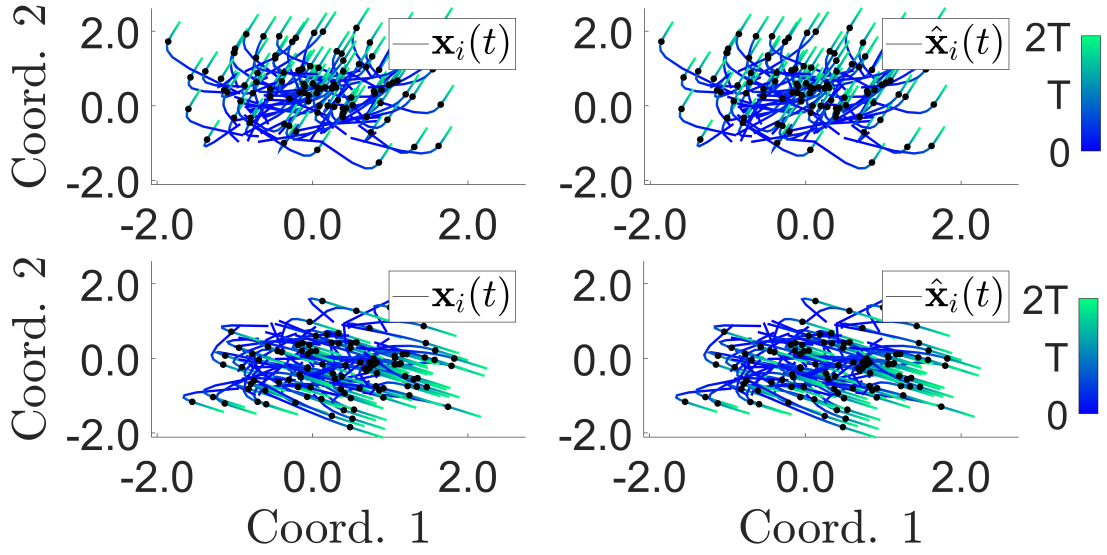


Fig. 9: Comparison of true (left) and predicted (right) agent trajectories using estimated interaction kernel  $\hat{\phi}$  with 10% noise. Despite local errors in  $\hat{\phi}$ , the predicted system behavior remains consistent with the ground truth.

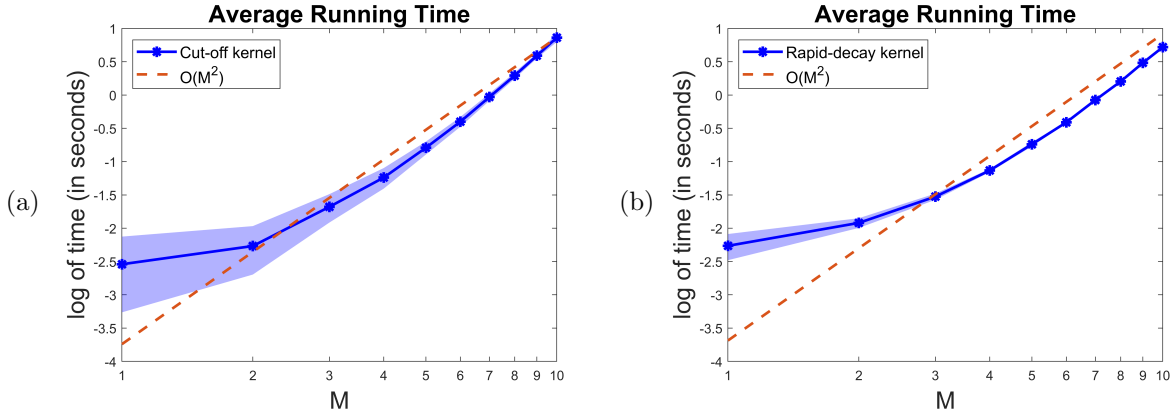


Fig. 10: Average running time for learning Cucker-Smale models with two different kernels.

As in the first-order opinion dynamics case, we report the average runtime of our algorithm under different dataset sizes for both kernel types (cut-off and rapid decay). As shown in Figure 10, the computational cost grows approximately as  $\mathcal{O}(M^2)$  in both cases, reflecting the practical benefits of the sparsity structure in the assembled regression matrices.

**5. Conclusion and Discussion.** This work presents a variational framework for learning asymmetric interaction kernels in the Motsch–Tadmor model using trajectory data. By reformulating the governing equations in implicit form, the inverse problem is reduced to a subspace identification task. We establish an identifiability result under suitable conditions on the data distribution and basis support, providing theoretical guarantees for kernel recovery.

To address ill-posedness and noise sensitivity, we develop a sparse Bayesian learning (SBL) algorithm

that incorporates prior structure, enables model selection via a new weighted total uncertainty (wTU) criterion, and provides uncertainty quantification. Numerical experiments demonstrate accurate recovery of interaction laws and robustness across noise levels and limited data.

Future work includes extensions to position-only observations, heterogeneous or time-varying interactions, and finite-sample recovery guarantees. The proposed framework contributes a principled, interpretable approach to data-driven modeling of asymmetric dynamical systems.

## REFERENCES

- [1] Juan A Acebrón, Luis L Bonilla, Conrad J Pérez Vicente, Félix Ritort, and Renato Spigler. The kuramoto model: A simple paradigm for synchronization phenomena. *Reviews of modern physics*, 77(1):137–185, 2005.
- [2] S Derin Babacan, Rafael Molina, and Aggelos K Katsaggelos. Bayesian compressive sensing using laplace priors. *IEEE Transactions on image processing*, 19(1):53–63, 2009.
- [3] S Derin Babacan, Rafael Molina, and Aggelos K Katsaggelos. Fast bayesian compressive sensing using laplace priors. In *2009 IEEE International Conference on Acoustics, Speech and Signal Processing*, pages 2873–2876. IEEE, 2009.
- [4] M. Ballerini, N. Cabibbo, R. Candelier, A. Cavagna, E. Cisbani, I. Giardina, V. Lecomte, A. Orlandi, G. Parisi, A. Procaccini, M. Viale, and V. Zdravkovic. Interaction ruling animal collective behavior depends on topological rather than metric distance: Evidence from a field study. *Proc Natl Acad Sci USA*, 105(4):1232–1237, 2008.
- [5] W. Bialek, A. Cavagna, I. Giardina, T. Mora, E. Silvestri, M. Viale, and A. M. Walzak. Statistical mechanics for natural flocks of birds. *Proc Natl Acad Sci USA*, 109:4786 – 4791, 2012.
- [6] Vincent D Blondel, Julien M Hendrickx, Alex Olshevsky, and John N Tsitsiklis. Convergence in multiagent coordination, consensus, and flocking. In *Proceedings of the 44th IEEE Conference on Decision and Control*, pages 2996–3000. IEEE, 2005.
- [7] Vincent D Blondel, Julien M Hendrickx, and John N Tsitsiklis. On krause’s multi-agent consensus model with state-dependent connectivity. *IEEE transactions on Automatic Control*, 54(11):2586–2597, 2009.
- [8] J. Bongard and H. Lipson. Automated reverse engineering of nonlinear dynamical systems. *Proceedings of the National Academy of Sciences of the United States of America*, 104(24):9943–9948, 2007.
- [9] L. Boninsegna, F. Nüske, and C. Clementi. Sparse learning of stochastic dynamical equations. *The Journal of Chemical Physics*, 148(24):241723, 2018.
- [10] S. Brunton, N. Kutz, and J. Proctor. Data-driven discovery of governing physical laws. *SIAM News*, 50(1), 2017.
- [11] S. Brunton, J. Proctor, and J. Kutz. Discovering governing equations from data by sparse identification of nonlinear dynamical systems. *Proceedings of the National Academy of Sciences of the United States of America*, 113(15):3932–3937, 2016.
- [12] Iain D Couzin, Jens Krause, Richard James, Graeme D Ruxton, and Nigel R Franks. Collective memory and spatial sorting in animal groups. *Journal of theoretical biology*, 218(1):1–11, 2002.
- [13] Felipe Cucker and Steve Smale. Emergent behavior in flocks. *IEEE Transactions on automatic control*, 52(5):852–862, 2007.
- [14] Borjan Geshkovski, Cyril Letrouit, Yury Polyanskiy, and Philippe Rigollet. The emergence of clusters in self-attention dynamics. *Advances in Neural Information Processing Systems*, 36, 2024.
- [15] Seung-Yeal Ha, Franca Hoffmann, Dohyeon Kim, and Wook Yoon. Mono-cluster flocking and uniform-in-time stability of the discrete motsch-tadmor model. *arXiv preprint arXiv:2408.10213*, 2024.
- [16] X. Han, Z. Shen, W. Wang, and Z. Di. Robust reconstruction of complex networks from sparse data. *Physical Review Letters*, 114(2):028701, 2015.
- [17] Pierre-Emmanuel Jabin and Sebastien Motsch. Clustering and asymptotic behavior in opinion formation. *Journal of Differential Equations*, 257(11):4165–4187, 2014.
- [18] Chunyin Jin. Flocking of the motsch-tadmor model with a cut-off interaction function. *Journal of Statistical Physics*, 171(2):345–360, 2018.
- [19] Kadierdan Kaheman, J Nathan Kutz, and Steven L Brunton. Sindy-pi: a robust algorithm for parallel implicit sparse identification of nonlinear dynamics. *Proceedings of the Royal Society A*, 476(2242):20200279, 2020.
- [20] S. Kang, W. Liao, and Y. Liu. Ident: Identifying differential equations with numerical time evolution. *arXiv preprint arXiv:1904.03538*, 2019.
- [21] Yael Katz, Kolbjørn Tunstrøm, Christos C Ioannou, Cristián Huepe, and Iain D Couzin. Inferring the structure and dynamics of interactions in schooling fish. *Proceedings of the National Academy of Sciences*, 108(46):18720–18725, 2011.
- [22] Evelyn F Keller and Lee A Segel. Model for chemotaxis. *Journal of theoretical biology*, 30(2):225–234, 1971.
- [23] Ulrich Krause. A discrete nonlinear and non-autonomous model of consensus formation. *Communications in difference equations*, 2000:227–236, 2000.
- [24] Dilip Krishnan and Rob Fergus. Fast image deconvolution using hyper-laplacian priors. *Advances in neural information processing systems*, 22, 2009.
- [25] Jacques Laskar. The chaotic motion of the solar system: A numerical estimate of the size of the chaotic zones. *Icarus*, 88(2):266–291, 1990.
- [26] Fanghui Liu, Xiaolin Huang, Yudong Chen, and Johan AK Suykens. Random features for kernel approximation: A survey on algorithms, theory, and beyond. *IEEE Transactions on Pattern Analysis and Machine Intelligence*, 44(10):7128–7148, 2021.

- [27] Z. Long, Y. Lu, X. Ma, and B. Dong. PDE-net: Learning PDEs from data. *arXiv preprint arXiv:1710.09668*, 2017.
- [28] Fei Lu, Mauro Maggioni, and Sui Tang. Learning interaction kernels in stochastic systems of interacting particles from multiple trajectories. *arXiv preprint arXiv:2007.15174*, 2020.
- [29] Fei Lu, Mauro Maggioni, and Sui Tang. Learning interaction kernels in heterogeneous systems of agents from multiple trajectories. *The Journal of Machine Learning Research*, 22(1):1518–1584, 2021.
- [30] Fei Lu, Ming Zhong, Sui Tang, and Mauro Maggioni. Nonparametric inference of interaction laws in systems of agents from trajectory data. *Proceedings of the National Academy of Sciences*, 116(29):14424–14433, 2019.
- [31] Ryan Lukeman, Yue-Xian Li, and Leah Edelstein-Keshet. Inferring individual rules from collective behavior. *Proceedings of the National Academy of Sciences*, 107(28):12576–12580, 2010.
- [32] Niall M Mangan, Steven L Brunton, Joshua L Proctor, and J Nathan Kutz. Inferring biological networks by sparse identification of nonlinear dynamics. *IEEE Transactions on Molecular, Biological and Multi-Scale Communications*, 2(1):52–63, 2016.
- [33] Jason Miller, Sui Tang, Ming Zhong, and Mauro Maggioni. Learning theory for inferring interaction kernels in second-order interacting agent systems. *arXiv preprint arXiv:2010.03729*, 2020.
- [34] Sebastien Motsch and Eitan Tadmor. A new model for self-organized dynamics and its flocking behavior. *Journal of Statistical Physics*, 144:923–947, 2011.
- [35] Sebastien Motsch and Eitan Tadmor. Heterophilous dynamics enhances consensus. *SIAM review*, 56(4):577–621, 2014.
- [36] Sebastien Motsch and Eitan Tadmor. Heterophilous dynamics enhances consensus. *SIAM Review*, 56(4):577–621, 2014.
- [37] Hegselmann Rainer and Ulrich Krause. Opinion dynamics and bounded confidence: Models, analysis and simulation. *Journal of Artificial Societies and Social Simulation*, 5(3), 2002.
- [38] M. Raissi. Deep hidden physics models: Deep learning of nonlinear partial differential equations. *The Journal of Machine Learning Research*, 19(1):932–955, 2018.
- [39] M. Raissi and G. Karniadakis. Hidden physics models: Machine learning of nonlinear partial differential equations. *Journal of Computational Physics*, 357:125–141, 2018.
- [40] S. Rudy, S. Brunton, J. Proctor, and N. Kutz. Data-driven discovery of partial differential equations. *Science Advances*, 3(4):e1602614, 2017.
- [41] Aditya Sant, Markus Leinonen, and Bhaskar D Rao. Block-sparse signal recovery via general total variation regularized sparse bayesian learning. *IEEE Transactions on Signal Processing*, 70:1056–1071, 2022.
- [42] Hayden Schaeffer, Giang Tran, and Rachel Ward. Extracting sparse high-dimensional dynamics from limited data. *SIAM Journal on Applied Mathematics*, 78(6):3279–3295, 2018.
- [43] M. Schmidt and H. Lipson. Distilling free-form natural laws from experimental data. *Science*, 324(5923):81–85, 2009.
- [44] Michael E Tipping. Sparse Bayesian learning and the relevance vector machine. *Journal of machine learning research*, 1(Jun):211–244, 2001.
- [45] Michael E Tipping and Anita C Faul. Fast marginal likelihood maximisation for sparse bayesian models. In *International workshop on artificial intelligence and statistics*, pages 276–283. PMLR, 2003.
- [46] G. Tran and R. Ward. Exact recovery of chaotic systems from highly corrupted data. *Multiscale Modeling and Simulation*, 15(3):1108–1129, 2017.
- [47] Tamás Vicsek, András Czirók, Eshel Ben-Jacob, Inon Cohen, and Ofer Shochet. Novel type of phase transition in a system of self-driven particles. *Physical review letters*, 75(6):1226, 1995.
- [48] David Wipf and Srikantan Nagarajan. Iterative reweighted  $\ell_1$  and  $\ell_2$  methods for finding sparse solutions. *IEEE Journal of Selected Topics in Signal Processing*, 4(2):317–329, 2010.
- [49] Sheng Zhang and Guang Lin. Robust data-driven discovery of governing physical laws with error bars. *Proceedings of the Royal Society A: Mathematical, Physical and Engineering Sciences*, 474(2217):20180305, 2018.
- [50] Zhilin Zhang and Bhaskar D Rao. Sparse signal recovery with temporally correlated source vectors using sparse bayesian learning. *IEEE Journal of Selected Topics in Signal Processing*, 5(5):912–926, 2011.